Battery Identification with Cubic Spline and Moving Horizon Estimation for Mobile Robots

Mohammad Shokri, Lorenzo Lyons, Sérgio Pequito, Laura Ferranti

***Abstract*—We propose a novel approach to track the state of charge (SoC) of batteries in mobile robots to improve their capabilities. The batteries' status is critical to accomplish their mission, but limited battery life can be a challenge. Our methodology focuses on modeling and estimating the SoC of batteries through system identification and fractional-order models. These models are flexible and can adjust to transient responses, allowing for accurate estimation of battery characteristics. Specifically, we use cubic spline interpolation to obtain the open circuit voltage (OCV) and the different resistors of the battery model. To estimate the SoC, we deploy a novel approach based on the moving horizon estimation (MHE) algorithm, which is suitable for handling poor initial estimation and constraints on the battery model. We consider the constraint on the peak discharging current, which can limit the performance of mobile robots in low-battery mode. We validate our approach by applying system identification and MHE to data from a mobile robot. The results show that our method accurately estimates the SoC despite poor initial values, enabling improved performance for mobile robots.**

***Index Terms*—Battery model, system identification, moving horizon estimation, fractional-order models, cubic spline.**

I. Introduction

Mobile robots have the potential to improve our quality of life in many applications such as warehouse logistics [1], scene reconstruction [2], and search-and-rescue [3]. To operate, mobile robots depend on their onboard battery. Thus, it is essential for mobile robots to monitor the battery's SoC in terms of percentage to fully charged to ensure the successful completion of their missions [4], [5].

Because there is no sensor for measuring the SoC directly, the SoC can be considered as a hidden state of the battery that has to be estimated based on the observed data from the battery, such as the terminal current and voltage. Therefore, it is crucial to have a reliable battery model to estimate the SoC through the current and voltage measurements. In particular, it is important for the mobile robot's batteries, which may have different behaviors connected to other electrical devices, such as motor drivers or electrical converters [6].

There are many data-driven approaches for modeling batteries that consider an electrochemical model whose parameters are obtained via system identification [7], [8]. Another approach is the equivalent circuit model (ECM), where the battery model consists of the open circuit voltage (OCV) and some electrical circuits to model the transient response [9], [4], [5]. In [9], the curve for the OCV is assumed to be available, and the authors obtain the parameters of the RC circuits. Especially, this assumption is essential for recursive least square approaches which are sensitive to initial conditions for compensating errors [10]. In [11], [12], a parametric model is considered for the OCV curve, which is made by some fixed functions. Toward a more flexible structure for the OCV, in [13], [14], the authors leverage a piece-linear interpolation that considers linear functions between every two consecutive points and can be fitted with data.

To model the temporal behavior of batteries, a chain of fixed RC circuits is exploited to model slow and fast transient responses [14], [15]. The work in [16], [17] considers RC circuits to depend on the SoC to model different temporal behavior in low-battery or high-battery modes. To extend the temporal flexibility, fractional-order calculus has attracted increasing interest for modeling batteries [18], [19]. In fractional-order models, fractional-order RC circuits (FRCCs) have been considered, in constant phase elements with fractional-order derivatives [20], [21]. Constant phase elements represent the electrochemical dynamics of the battery and can behave like ideal capacitors or resistors depending on their order of derivatives [22].

Given the battery model, there are a variety of approaches for estimation the SoC. The extended Kalman filter (EKF) is a popular method for SoC estimation because of the non-linearity of the battery model [23], [24]. An unscented Kalman filter (UKF) is also useful for estimating SoC since it can estimate the mean and covariance of error more accurately than EKF [4]. In [19], UKF is used for the fractional-order battery model. However, EKF and UKF misperform when the initial value of the estimation is far from the real value of SoC [25]. Also, they cannot handle the constraints and may estimate an infeasible SoC. An intrinsic limitation exists on the maximum deliverable power that is reduced in low-battery mode, and the battery cannot provide any current while it is in low-battery mode [26], [27]. Thus, the constraint on SoC and the peak current should also be considered in the SoC estimation [11], [16], [26], [27].

Moving horizon estimation (MHE) is an estimation method that is able to cope with the aforementioned issues faced by Kalman-based estimations such as EKF or UKF. Specially, MHE solves a constrained optimization problem to estimate SoC in a time-receding fashion. The works in [7], [8], [25] apply MHE to the battery model with the integer-order model.

M. Shokri, L. Lyons, L. Ferranti are with the Faculty of Mechanical, Maritime, and Material Engineering, Delft University of Technology, Delft, The Netherlands (email: {M.Shokri, L.Lyons, L.Ferranti}@tudelft.nl).

S. Pequito is with the Department of Information Technology at Uppsala University, Uppsala, Sweden (email: sergio.pequito@it.uu.se).

This work is supported by the Dutch Science Foundation NWO-TTW, within the Veni project HARMONIA (nr. 18165).

In this paper, we exploit MHE for a fractional-order battery model to consider the dynamics of FRCC and to factor in the low-battery mode constraint. In particular, we propose a fractional-order battery model with flexible structures for a SoC-OCV curve, a resistor, and multiple FRCCs whose resistors depend on the SoC to consider different behaviors in the SoC range.

To characterize the dependencies of SoC, the OCV and the resistance (of the resistor and the FRCCs) are considered to be curves of SoC. For curve formulation, we utilize cubic splines, which apply cubic polynomials between each pair of consecutive points to produce smooth and differentiable curves [28]. This method imbues our model with exceptional flexibility, enabling it to adeptly adjust to various environmental conditions. Then, we investigate the peak discharging current of the battery based on the available data. Afterward, given the battery model, we propose a MHE framework for the SoC and FRCCs' states by considering the SoC range constraints and the constraint of the peak discharging current. MHE minimizes the errors of the terminal voltage, the SoC dynamics, and the truncation errors made by fractional-order states.

The paper's contributions are the following:

- Application of fractional-order calculus to model a mobile robot's battery, including SoC-dependent curves for the OCV, resistor, and FRCCs, with higher description capabilities and, therefore, more flexible to perform system identification capturing the temporal behavior.
- Using splines to characterize the curves with smooth functions, which leads to flexible system identification.
- Inclusion of the peak discharging current of the battery when estimating SoC, allowing for a more comprehensive evaluation of battery performance.
- Design of a MHE algorithm for SoC estimation from a fractional-order model, which provides an effective method for handling poor initial estimation and constraints on the battery model.

The paper is structured as follows: Section II presents the preliminary information. Section III contains the battery model and its peak discharging current. Section IV proposes the system identification. Section V details the MHE for the battery model. Section VI presents the numerical results. Finally, Section VII concludes the remarks of the paper.

II. Preliminary

Our method relies on fractional-order calculus. In the following, we summarize its main results we will use in the paper. Fractional-order calculus extends the derivatives to an arbitrary (possibly fractional) order (e.g., Riemann-Liouville, Caputo, or Grünwald-Letnikov [29]). Hereafter, at time t, we consider the Grünwald-Letnikov definition with the α derivative of signal $u^t \in \mathbb{R}$ that can be define as follows

$$\mathcal{D}^{\alpha} u^t = \lim_{h \to 0} \frac{1}{h^{\alpha}} \sum_{k=0}^{\infty} \frac{(-1)^k \Gamma(\alpha+1)}{\Gamma(k+1)\Gamma(\alpha-k+1)} u^{t-k}, \quad (1)$$

where $\Gamma(.)$ is Gamma function defined as $\Gamma(n) = \int_0^{\infty} x^{n-1} e^{-x} dx$. In order to discretize (1), the sampling time δ is considered to be fixed. Thus, the discrete Grünwald-Letnikov is defined as follows

$$\mathcal{D}_{\delta}^{\alpha} u^t = \frac{1}{\delta^{\alpha}} \sum_{k=0}^{\infty} \frac{(-1)^k \Gamma(\alpha+1)}{\Gamma(k+1)\Gamma(\alpha-k+1)} u^{t-k}. \quad (2)$$

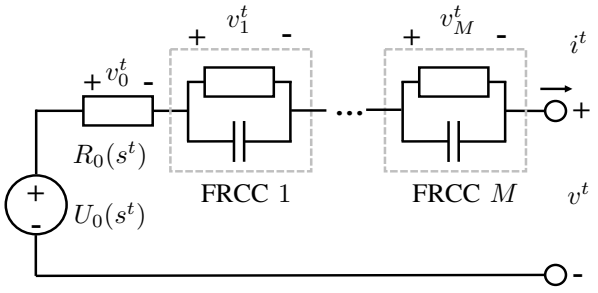

Fig. 1: Schematic of battery model comprising OCV, a resistor, and M FRCCs.

III. Battery Model

A. Battery Circuitry

Let $v^t \in \mathbb{R}$ and $i^t \in \mathbb{R}$ denote the terminal voltage and current of the battery, respectively. To characterize the charge level of the battery, we define $s^t \in [0,1]$ as the SoC of the battery at time $t \in \mathbb{N}$ that is calculated as follows:

$$s^{t+1} = s^t - \frac{\delta}{C} i^t + w_s^t, \quad (3)$$

where $\delta > 0$ is the sampling time, and $C > 0$ is the capacity of the battery. Additionally, $w_s^t \in \mathbb{R}$ stands for the disturbance affecting the SoC's dynamics at time t.

To model the battery, we use the circuitry that is illustrated in Figure 1. The battery model consists of an OCV, a resistor, and multiple FRCCs. The OCV is denoted by $U_0(s^t) \geq 0$ and depends on the SoC of the battery s^t at time t. The resistive circuit has the SoC-dependent resistance $R_0(s^t) \geq 0$, and its voltage is computed by $v_0^t = R_0(s^t) i^t$. Additionally, there are M FRCCs that are responsible for characterizing the transient response of the battery. Let $v_m^t \in \mathbb{R}$ and $i_m^t \in \mathbb{R}$ denote the voltage and the current of the $m \in \{1, \ldots, M\}$ FRCC, respectively. The evolution of voltage and current across the FRCC m is described by

$$\begin{aligned} i_m^t + \tau_m \mathcal{D}_{\delta}^{\alpha_m} i_m^t &= i^t, \\ v_m^t &= R_m(s^t) i_m^t, \end{aligned} \quad (4)$$

where $0 < \alpha_m < 2$ is the order of the derivative, and $\tau_m > 0$ is the time constant of FRCC m. Additionally, $R_m(s^t) \geq 0$ stands for the resistance of FRCC m, and $\mathcal{D}_{\delta}^{\alpha_m} i_m^t$ indicates the discrete Grünwald-Letnikov fractional-order derivative of $i_m^t \in \mathbb{R}$. Hereafter, we consider a truncation K of the discrete Gr¨unwald-Letnikov fractional-order as

$$\mathcal{D}_{\delta}^{\alpha_m} i_m^t = \frac{1}{\delta^{\alpha_m}} \sum_{k=0}^{K} \gamma_{m,k} i_m^{t-k} + e_{m,K}^t, \quad (5)$$

where $\gamma_{m,k} = \frac{(-1)^k \Gamma(\alpha_m+1)}{\Gamma(k+1)\Gamma(\alpha_m-k+1)}$ and $e_m^t = \frac{1}{\delta^{\alpha_m}} \sum_{k=K}^{\infty} \gamma_{m,k} i_m^{t-k}$. The error introduced by the

truncation is negligible for a sufficiently large $K \in \mathbb{N}$ since $|\gamma_{m,k}| \leq \frac{(\alpha_m)^K}{K!}$ [30]. Therefore, we can re-write (4) as

$$i_m^t + \frac{\tau_m}{\delta^{\alpha_m}} \sum_{k=0}^{K-1} \gamma_{m,k} i_m^{t-k} + \tau_m e_{m,K}^t = i^t. \tag{6}$$

Based on (3) and (4), the terminal voltage is obtained as

$$v^t = U_0(s^t) - R_0(s^t) i^t - \sum_{m=1}^{M} R_m(s^t) i_m^t + w_v^t, \tag{7}$$

where w_v^t stands for the noise of the terminal voltage.

B. Cubic Spline

The battery model (7) depends on the functions $U_0(s^t)$, $R_0(s^t)$, and $R_m(s^t)$ that depend on the SoC. To characterize these functions, we use their interpolation via cubic spline with $N+1$ points to assure continuity for the first and second derivative [31], [32]. Let us consider partitioning the interval $[0, 1]$ into $N \in \mathbb{N}$ equally sized intervals by $x_n = n/N$ for $n = 0, \ldots, N$. Then, for $s^t \in [x_n, x_{n+1}]$, we have

$$\begin{aligned} U_0(s^t) =& h_n^U P(N(s^t - x_n)) + h_{n+1}^U P(N(x_{n+1} - s^t)) \\ &+ y_n^U (N(s^t - x_n)) + y_{n+1}^U (N(x_{n+1} - s^t)), \\ R_0(s^t) =& h_n^0 P(N(s^t - x_n)) + h_{n+1}^0 P(N(x_{n+1} - s^t)) \\ &+ y_n^0 (N(s^t - x_n)) + y_{n+1}^0 (N(x_{n+1} - s^t)), \\ R_m(s^t) =& h_n^m P(N(s^t - x_n)) + h_{n+1}^m P(N(x_{n+1} - s^t)) \\ &+ y_n^m (N(s^t - x_n)) + y_{n+1}^m (N(x_{n+1} - s^t)), \end{aligned} \tag{8}$$

where $P(x) = \frac{1}{6}(x^3 - x)$. For $n = 0, \ldots, N$, it follows that y_n^U, y_n^0, and y_n^m are the values of the functions at $s^t = x_n$. Similarly, for $n = 0, \ldots, N$, we have h_n^U, h_n^0, and h_n^m parameters whose zero value indicates that the second derivative of the function is zero at $s^t = x_n$. Since $U_0(s^t)$, $R_0(s^t)$, and $R_m(s^t)$ are non-negative, we have:

$$y_n^U \geq 0, \quad y_n^0 \geq 0, \quad y_n^m \geq 0, \tag{9}$$

for $n = 0, \ldots, N$ and $m = 1, \ldots, M$. To ensure continuity in the first derivative, the following constraints must hold:

$$\begin{aligned} 0.5h_{n-1}^U + 2h_n^U + 0.5h_{n+1}^U &= 3(y_{n-1}^U - 2y_n^U + y_{n+1}^U), \\ 0.5h_{n-1}^0 + 2h_n^0 + 0.5h_{n+1}^0 &= 3(y_{n-1}^0 - 2y_n^0 + y_{n+1}^0), \\ 0.5h_{n-1}^m + 2h_n^m + 0.5h_{n+1}^m &= 3(y_{n-1}^m - 2y_n^m + y_{n+1}^m), \end{aligned} \tag{10}$$

for $n = 1, \ldots, N-1$. For the boundary conditions (i.e., $n \in \{0, N\}$), we can assume that

$$h_0^U = h_N^U = h_0^0 = h_N^0 = h_0^m = h_N^m = 0. \tag{11}$$

Intuitively, the condition (11) implies that $U_0(s^t)$, $R_0(s^t)$, and $R_m(s^t)$ have more linear traits on the boundaries.

C. Peak Discharging Current

In this section, we delve into the examination of the battery's peak discharging current, a critical factor in governing the mobile robot's operations and orchestrating their tasks during low-battery scenarios. Every battery has a threshold for the maximum power it can deliver, and this constraint

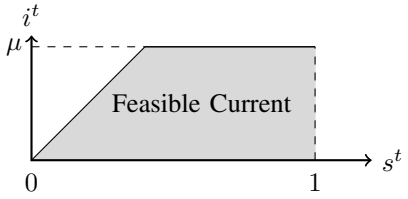

Fig. 2: Peak discharging current.

plays a pivotal role in overseeing the battery of mobile robots and strategizing their missions. Moreover, when estimating the SoC, the peak discharging current defines a viable range beyond which achieving specific SoC values becomes unattainable. It is imperative that the estimated SoC values adhere to the constraints associated with the peak discharging current.The peak discharging current depends on the SoC [27]. Specifically, at a lower charge, it has a linear dependency

$$i^t \leq \gamma s^t, \tag{12}$$

where $\gamma > 0$. Furthermore, the current does not exceed the constant μ, i.e., $i^t \leq \mu$. Figure 2 depicts the feasible region for the terminal current.

IV. System Identification

Given the battery model, this section describes the model's cubic splines to meet the battery's voltage and current data. To this end, we use a dataset from the terminal voltage and current for system identification. We aim to identify the parameters of the cubic splines regarding OCV, the resistor, and FRCCs' resistor, i.e., y_n^U, y_n^0, y_n^m, h_n^U, h_n^0, and h_n^m. Plus, we determine the parameters of the peak discharging current with the data.

On our dataset, $v^{t,q}$ and $i^{t,q}$ are available for trial $q = 1, \ldots, Q$ at $t = 1, \ldots, T_q$. Given α_m and τ_m, we can calculate $i_m^{t,q}$ time series for $m = 1, \ldots, M$ via (6). The trials start from the full-charge situation, and based on the initial SoC of each trial, we can calculate $s^{t,q}$ via Coulomb counting from (3). Let z^{SI} stand for the vector that concatenates the variables y_n^U, y_n^0, y_n^m, h_n^U, h_n^0, and h_n^m, for $n = 0, \ldots, N$ and $m = 1, \ldots, M$. Given the data from $v^{t,q}$, $i^{t,q}$, and $s^{t,q}$, the following optimization to obtain the cubic spline parameters

$$\begin{aligned} \min_{z^{SI}} & \sum_{q=1}^{Q} \sum_{t=1}^{T_q} \left\| v^{t,q} - U_0(s^{t,q}) + R_0(s^{t,q}) i^{t,q} + \sum_{m=1}^{M} R_m(s^{t,q}) i_m^{t,q} \right\|^2 \\ &+ \sum_{n=0}^{N} (\lambda^U |h_n^U| + \lambda^0 |h_n^0| + \lambda^m |h_n^m|) \\ & \textbf{s.t.} \ (8), (9), (10), \text{ and } (11) \text{ for } n = 0, \ldots, N, \\ & m = 1, \ldots, M, \text{ and } q = 1, \ldots, Q. \end{aligned} \tag{13}$$

where λ^U, λ^0, and λ^m are hyperparameters. The term $\sum_{n=0}^{N} (\lambda^U |h_n^U| + \lambda^0 |h_n^0| + \lambda^m |h_n^m|)$ has a regularization role for the system identification to promote a lower second derivative. Specifically, the absolute value may lead some of h_n^U, h_n^0, and h_n^m to be zero, which shows the tendency of (13) to obtain the linear curves for $U_0(s^t)$, $R_0(s^t)$, and $R_m(s^t)$ at each point.

Algorithm 1 System identification for modeling battery

Inputs
Time series of $v^{t,q}$ and $i^{t,q}$ for $q = 1, \dots, Q$ at $t = 1, \dots, T_q$
α_m and τ_m for $m = 1, \dots, M$
λ^U, λ^0, and λ^m

SoC
Calculate $s^{t,q}$ from (3) for each trial $q = 1, \dots, Q$ at $t = 1, \dots, T_q$

FRCC
Calculate $i_m^{t,q}$ from (4) and (5) for $m = 1, \dots, M$ and $q = 1, \dots, Q$ at $t = 1, \dots, T_q$

System Identification
Solve the optimization problem (13)

Based on (8), $U_0(s^{t,q})$, $R_0(s^{t,q})$, and $R_m(s^{t,q})$ have a linear dependency on the optimization parameters. Therefore, the cost function in (13) is convex with respect to the optimization parameters. Moreover, (9), (10), and (11) are linear constraints with respect to the optimization parameters. Therefore, (13) is a convex optimization and has a unique solution. Algorithm 1 provides the procedure for system identification in (13).

The constraint in (12) shows the limitation on the terminal current. To determine μ and γ, we assume a dataset containing adequate situations with extracting peak current for the whole range of SoC. Thus, they can be computed by $\mu = \max i^{t,q}$ and $\gamma = \max \frac{i^{t,q}}{s^{t,q}}$, with $q = 1, \dots, Q$ and $t = 1, \dots, T_q$.

V. Moving Horizon Estimation

The battery model has hidden states, such as the SoC or the FRCCs' current, which cannot be measured directly. Given an identified battery model, we design a state estimator from the observed data of terminal voltage and current via MHE.

Let us assume the time series of the terminal voltage (v^t) and terminal current (i^t) are available. To this end, we use MHE to estimate states based on a sequence of H past measurements. Let us define $H^t = \mathbf{min}\{H, t\}$ to handle the MHE at the initial stage where the available samples are less than H. Suppose $v^{(t-H^t):t} = [v^{t-H^t}, \dots, v^t]^\top$ and $i^{(t-H^t):t} = [i^{t-H^t}, \dots, i^t]^\top$ be the observed sequence of terminal voltage and current, respectively. Also, suppose that $\hat{s}^{t-H^t}$ and $\hat{i}_m^{t-H^t}$ are the available estimation of s^{t-H^t} and $i_m^{t-H^t}$, respectively. Let us define $\tilde{s}^{(t-H^t):t} = [\tilde{s}^{t-H^t}, \dots, \tilde{s}^t]^\top$ and $\tilde{i}_m^{(t-H^t):t} = [\tilde{i}_m^0, \dots, \tilde{i}_m^{H^t+1}]^\top$ as optimization variables corresponding to a sequence of s^t and i_m^t, respectively.

Based on the dynamics of the SoC in (3), we have the following constraints

$$\begin{aligned} &\tilde{s}^{t'+1} = \tilde{s}^{t'} - \frac{\delta}{C} i^{t'} + \tilde{w}_s^{t'}, \text{ for } t - H^t \le t' \le t-1, \\ &0 \le \tilde{s}^{t'} \le 1, i^{t'} \le \gamma \tilde{s}^{t'}, \text{ for } t - H^t \le t' \le t. \end{aligned} \tag{14}$$

Let us denote $\tilde{w}_s^{(t-H^t):(t-1)} = [\tilde{w}_s^{t-H^t}, \dots, \tilde{w}_s^{t-1}]^\top$. Moreover, according to (6), we have the following constraints

$$\tilde{i}_m^{t'} + \tau_m \sum_{k=0}^{t-H^t-t'} \gamma_{m,k} \tilde{i}_m^{t'-k} + \tau_m \tilde{e}_m^{t'} = i^{t'}, \tag{15}$$

for $t - H^t \le t' \le t$. Let us denote $\tilde{e}_m^{(t-H^t):t} = [\tilde{e}_m^{t-H^t}, \dots, \tilde{e}_m^t]^\top$. Note that (15) uses different truncations for different t' because we only use the terminal current's data for the estimation in the interval $t - H^t$ to t.

Based on (7), for the voltage measurements, we have the following constraint:

$$v^{t'} = U_0(\tilde{s}^{t'}) - R_0(\tilde{s}^{t'}) i^{t'} - \sum_{m=1}^{M} R_m(\tilde{s}^{t'}) \tilde{i}_m^{t'} + \tilde{w}_v^{t'}, \tag{16}$$

for $t - H \le t' \le t$. Let us denote $\tilde{w}_v^{(t-H^t):t} = [\tilde{w}_v^{t-H^t}, \dots, \tilde{w}_v^t]^\top$. It would be difficult to use (16) as constraints since it is not linear with respect to $\tilde{s}^{t'}$. Therefore, we linearize (16) around $s = \hat{s}^{t-H^t}$ as

$$v^{t'} = u_0 + l_0 \tilde{s}^{t'} - r_0 i^{t'} - \sum_{m=1}^{M} r_m \tilde{i}_m^{t'} + \tilde{w}_v^{t'}, \tag{17}$$

where

$$\begin{aligned} &u_0 = U_0(\hat{s}^{t-H^t}), l_0 = \frac{\partial U_0}{\partial s}(\hat{s}^{t-H^t}), \text{ and} \\ &r_0 = R_0(\hat{s}^{t-H^t}), r_m = R_m(\hat{s}^{t-H^t}). \end{aligned} \tag{18}$$

Let $z^{MHE,t}$ stand for the vector that concatenates the variables $\tilde{s}^{(t-H^t):t}$, $\tilde{i}_m^{(t-H^t):t}$, $\tilde{w}_s^{(t-H^t):(t-1)}$, $\tilde{w}_v^{(t-H^t):t}$, and $\tilde{e}_m^{(t-H^t):t}$ for $m = 1, \dots, M$. By defining the constraints, the MHE is formulated as follows:

$$\begin{aligned} \min_{z^{MHE,t}} \; & p_s ||\tilde{s}^{t-H^t} - \hat{s}^{t-H^t}||^2 + \sum_{m=1}^{M} p_{i,m} ||\tilde{i}_m^{t-H^t} - \hat{i}_m^{t-H^t}||^2 \\ & + ||\tilde{w}_s^{(t-H^t):(t-1)}||^2_{P_s} + ||\tilde{w}_v^{(t-H^t):t}||^2_{P_v} \\ & + \sum_{m=1}^{M} ||\tilde{e}_m^{(t-H^t):t}||^2_{P_{i,m}} \\ \textbf{s.t.} \; & (14), (15), \text{ and } (17) \text{ for } m = 1, \dots, M, \end{aligned} \tag{19}$$

where p_s and $p_{i,m}$ are the weights of the initial estimation terms that lead $\tilde{s}^{t-H^t}$ and $\tilde{i}_m^{t-H^t}$ to be obtained close to the last estimations (i.e., $\hat{s}^{t-H^t}$ and $\hat{i}_m^{t-H^t}$) at the beginning of the interval. The matrices P_s, P_v, and $P_{i,m}$ are the weights of different cost function terms.

Algorithm 2 shows the procedure of MHE. The MHE is initiated with the initial estimates $\hat{s}^0$ and $\hat{i}_m^0$ for $m = 1, \dots, M$. At time t, the optimal values of $\tilde{s}^{(t-H^t):t}$ and $\tilde{i}_m^{(t-H^t):t}$ are calculated based on the last estimations $\hat{s}^{t-H^t}$ and $\hat{i}_m^{t-H^t}$ for $m = 1, \dots, M$ on the horizon $(t - H^t)$ to t. Afterwards, $\hat{s}^{t-H^t+1}$ and $\hat{i}_m^{t-H^t+1}$ are updated with the optimal values of corresponding elements $z^{MHE,t}$ from the optimization (19).

An advantage of MHE is that it can account for constraints in the estimation problem. There are two types of inequality constraints in our proposed solution (see Algorithm 2): (i) the SoC range and (ii) the peak discharging current. Based on

Algorithm 2 MHE for battery model at time t

Inputs

Estimation horizon H

p_s, $p_{i,m}$, P_s, P_v, and $P_{i,m}$ for $m = 1, \dots, M$

The initial estimations $\hat{s}^0$ and $\hat{i}_m^0$ for $m = 1, \dots, M$

For time $t \geq 0$

$H^t = \mathbf{min}\{H, t\}$

$v^{(t-H^t):t} = [v^{t-H^t}, \dots, v^t]^\top$

$i^{(t-H^t):t} = [i^{t-H^t}, \dots, i^t]^\top$

Linearization

Calculate u_0, l_0, r_0, and r_m by (18) for $m = 1, \dots, M$

MHE

Solve the optimization problem (19)

Update $\hat{s}^{t-H^t+1}$ and $\hat{i}_m^{t-H^t+1}$ for $m = 1, \dots, M$

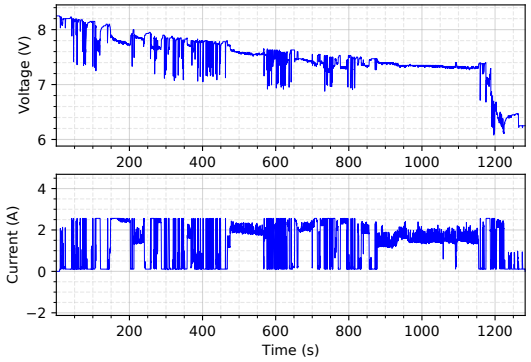

Fig. 3: Voltage and current time series for a trial.

the SoC range and the nature of the battery, it is impossible to violate these constraints, e.g., SoC more than 1 or high current in low-battery mode. The constraints in MHE are responsible for forcing the estimation to be in the feasible region.

VI. Numerical Results

A. Mobile Robot Data

To evaluate the methodology, we apply the algorithms to the battery data of a mobile robot in 5 trials. Figure 4 shows the mobile robot used for the experiments. For each trial, the robot starts in a fully charged state. Then, it moves and stops frequently to deplete the battery. The robot's battery is a two-cell rechargeable polymer lithium-ion battery with a 550 mAh capacity with a usable voltage range of $3.2V$ to $4.2V$ per cell. The trials are divided into two sets of training (4 trials) and testing (1 trial) results. Figure 3 shows the terminal voltage and current time series of the battery for the training data. Notice that the terminal voltage and current have many sharp peaks and drops due to the route that the mobile robot follows. Also, the current drops at the end of the experiment because of the limitations on low-battery mode.

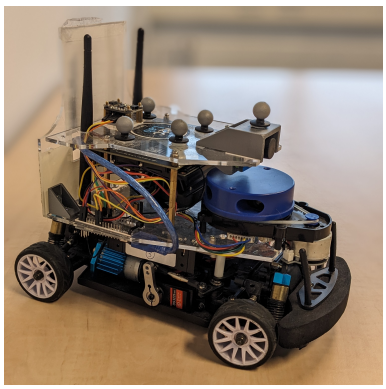

Fig. 4: The mobile robot.

B. System Identification

For system identification, we use the training data, and we calculate the state of charge via Coulomb counting from (3) and using the assumption that the trial starts from fully-charged mode. For the system identification, we consider a battery model with one FRCC with $\alpha_1 = 1.2$ and $\tau_1 = 0.05s$. We considered $N = 21$ points regarding $U_0(s^t)$, $R_0(s^t)$, and $R_1(s^t)$. The hyperparameters λ^U, λ^0, and λ^1 are considered to be 15, 150, and 100, respectively. The truncation sample size for fractional-order calculation is considered as $K = 10$.

The parameters of the battery model are determined using by Algorithm 1. To evaluate the model, we use cross-validation on the testing data. Figure 5 shows the terminal voltage, its prediction, and its error. The predicted voltage follows the trend of the real terminal voltage, and the model follows the battery's behavior well. The prediction error does not exceed $0.25V$ (35% of the terminal voltage). The prediction percent error (PE^t) at time t is defined as $PE^t = 100\frac{|v^t - \hat{v}^t|}{v^t}$ where v^t and $\hat{v}^t$ are real and predicted voltages, respectively. Our model's average percent error (the percentage of prediction error to the real value) is approximately 0.53%. However, it might be possible to get less error upon fine tunning some of the parameters. Also, the parameters μ and γ are equal to $2.6A$ and $11.9A$, respectively.

Figure 6 shows the OCV determined by our proposed method as described in Section IV. The system identification smoothly calculates the OCV curve. Although there are $N = 21$ points for interpolation of the curve, the curve stays smooth as much as possible because of the regularization term $\sum_{n=0}^{N} \lambda^U |h_n^U|$. This regularization decreases the curvature of the splines at each interpolation point so that the curve remains linear as far as it is possible. The OCV drops when SoC is close to 0.28. Also, we have less change in OCV in the middle range than in the high range of SoC.

Figure 7 displays the resistance curves for the resistor and the FRCC. Similar to the OCV curve, these curves are obtained smoothly with less fluctuation because of the regularization terms in the system identification. Contrary to the pulse-based experiments for determining resistance parameters as in [16], [17], our method employs data-driven techniques that leverage natural terminal current fluctuations. This strategy proves especially beneficial for mobile robots, given the integration

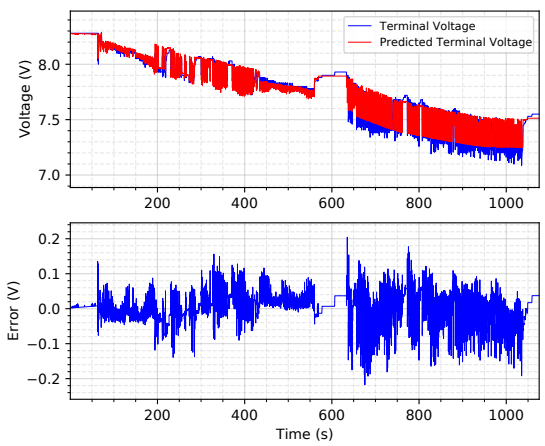

Fig. 5: Terminal voltage prediction and prediction error on testing data.

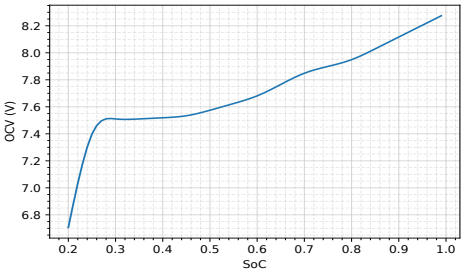

Fig. 6: OCV curve obtained by the system identification.

of the battery with diverse circuits, such as motor drivers. By utilizing direct observations, our method streamlines the estimation process, enhancing its relevance to the practical operation of mobile robots. Moreover, this approach facilitates the scalability and deployability of mobile robots in real-world environments, underscoring its practical advantages.

Table I depicts the performance of the modeling with respect to the fractional order of the derivative via average percent error. The average percent error has its lowest value on $\alpha_1 = 1.2$. Specially, when $\alpha_1 = 1$ (integer order model), we have higher errors than with $\alpha_1 = 1.2$, which shows the advantage of using fractional-order models. Also, we repeated the simulations for two FRCCs, and as shown in Table I, the fractional-order systems can perform better than multiple integer order elements for describing the temporal behavior.

TABLE I: Average percent error of the system identification with respect to the order of fractional derivative.

	Single FRCC	Double FRCCs	
		$\alpha_2 = 1$	$\alpha_2 = 1.1$
$\alpha_1 = 0.9$	1.23%	1.92%	1.57%
$\alpha_1 = 1.0$	0.91%	1.21%	1.03%
$\alpha_1 = 1.1$	0.62%	0.87%	0.71%
$\alpha_1 = 1.2$	0.53%	0.63%	0.58%
$\alpha_1 = 1.3$	0.57%	0.68%	0.61%

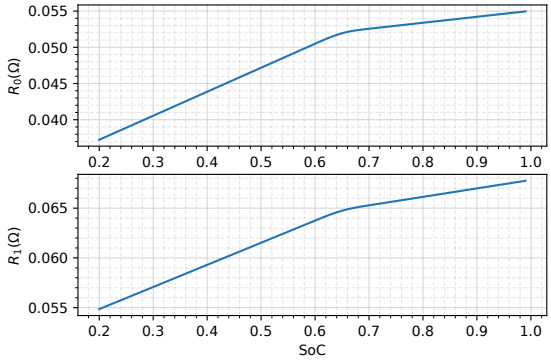

Fig. 7: Resistance curve for resistive circuit and FRCC obtained from system identification.

C. MHE

Assuming that the terminal current and voltage are available, MHE exploits the identified battery model to estimate the SoC and the current of the FRCC. We consider $H = 20$ for the horizon of the MHE. The hyperparameters are considered as follows: $p_s = 1000$, $p_{i,1} = 1000$, $P_s = 100000 I_H$, $P_v = I_H$, and $P_{i,1} = 0.1 I_H$ where I_H is identity matric with size $H \times H$. The truncation sample size is considered to be $K = 10$ for the discretized fractional-order dynamics.

As a ground-truth, to validate the MHE, we used synthetic data that are artificially generated by simulation. To do so, we extract the current time series of training data from the model and set 1 for the initial SoC. The synthetic data contains the simulation values for the states (SoC and the current of FRCC) that can be compared with the estimated states. For MHE, we consider two different values of the initial SoC of the estimation: $\tilde{s}^0 = 0.9$, $\tilde{s}^0 = 0.5$, EKF (for $\tilde{s}^0 = 0.5$), and UKF (for $\tilde{s}^0 = 0.5$). Figure 8a shows the synthetic data and the results of MHE for the two aforementioned cases. In particular, the estimates of SoC converge to the synthetic SoC. In contrast with EKF and UKF, MHE converges quickly to the synthetic SoC regardless of different initial estimations. Also, Table II compares the sensitivity of the methods to initial estimation. MHE has less error compared to the other methods to compensate for the poor initial estimation. That provides evidence of an advantage of MHE in coping with a poor initial value of the SoC.

TABLE II: Average absolute error of the estimation methods with respect to the initial estimated SoC.

$\tilde{s}^0$	MHE	EKF	UKF
0.9	0.0023	0.0028	0.0024
0.8	0.0025	0.0057	0.0048
0.7	0.0028	0.0142	0.0115
0.6	0.0032	0.0356	0.0223
0.5	0.0035	0.0486	0.0314

Figure 8b depicts the estimation results for the current of the FRCC from the synthetic data for the two aforementioned cases. Although the initial condition for the FRCC's current is the same, the estimations have some errors in the initial stage of the trajectory. The error happens in light of the poor initial

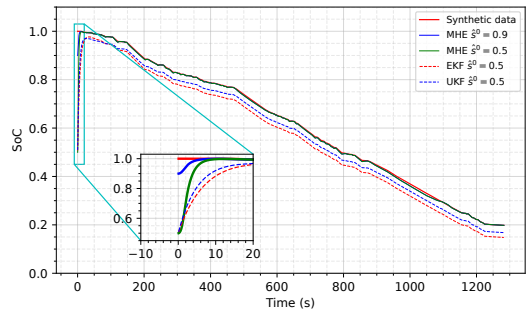

(a) Estimation of SoC.

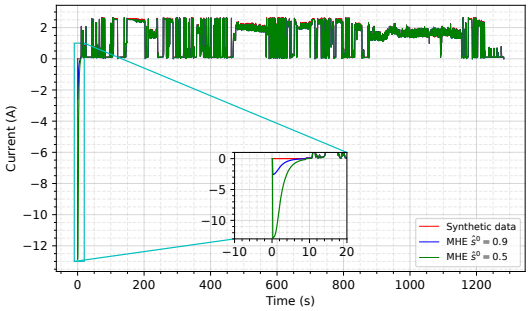

(b) Estimation of the FRCC's current.

Fig. 8: MHE from the synthetic data for $\tilde{s}^0 = 0.9$ and $\tilde{s}^0 = 0.5$ cases. Also, (a) shows the EKF and UKF estimation results (implemented based on [33]) from the synthetic data with initial value $\tilde{s}^0 = 0.5$.

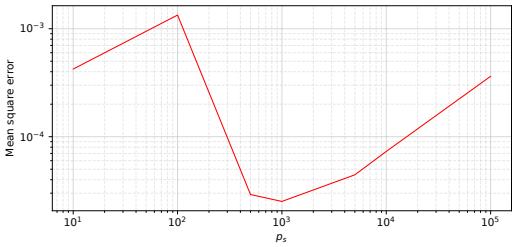

Fig. 9: Mean square error of MHE with respect to p_s.

condition of the SoC. However, the MHE compensates for the error with almost $8s$.

The quality of MHE depends on the parameters in the optimization (19). Figure 9 displays the mean square error of MHE and synthetic data with respect to p_s. p_s determines how much MHE relies on the previous estimation for the next estimation. The less p_s is, the noisier the results are obtained because MHE tends to estimate regardless of the previous estimations. Notice that the big values of p_s make MHE dependent on previous estimations, leading to slow estimation.

To validate the MHE on real data, we feed MHE with the test data and compare the results with Coulomb counting. Coulomb counting results can be interpreted as the deterministic battery model, i.e., by considering (3) with zero noise in SoC. Note that Coulomb counting neglects the stochasticity of

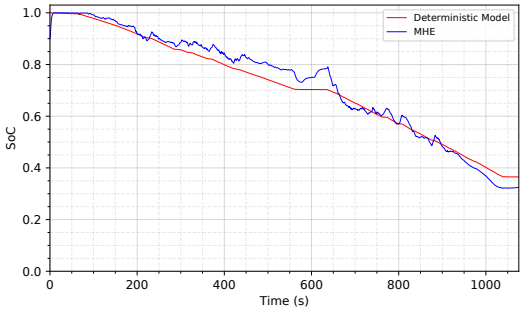

Fig. 10: Estimation of SoC for MHE and Coulomb counting (the deterministic battery model) from test data.

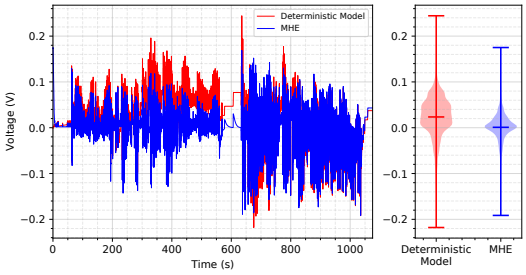

Fig. 11: Estimation the terminal voltage error and its distributions for MHE and Coulomb counting (the deterministic battery model) from test data. The ticks on the violin plot show the minimum, maximum, and mean of the errors

the battery and is not a ground-truth for the estimation. The SoC's initial value is set at 0.9. Figure 10 shows the estimation of SoC with MHE and Coulomb counting. Notice that the trajectories follow each other with an average and maximum absolute error of 0.04 and 0.08, respectively (after the transient stage). The difference between these two trajectories is due to the stochastic nature of the battery, the system identification error, and the MHE's error.

Figure 11 depicts the estimation error of the measured voltage for MHE and the deterministic model. The errors are calculated by subtracting the terminal voltage of the real data from the estimated voltages calculated by evaluating the estimated states in (7). Figure 11 shows the errors' distributions, and in particular, notice that MHE is closer to zero.

VII. Conclusion

This research paper proposes a novel methodology for system identification and state estimation of batteries in mobile robots. Our approach employs fractional-order components for increased temporal flexibility and cubic spline interpolation to obtain smooth curves for open circuit voltage and resistors. We also consider the limitation on peak discharging voltage to achieve a well-defined optimization problem for the moving horizon estimation algorithm used for state of charge estimation. Our methodology is validated through numerical results obtained from voltage and current data of a mobile robot, demonstrating the effectiveness of the system identification

and moving horizon estimation in accurately estimating the state of charge even with poor initial values.

Future research will aim to enhance our framework by incorporating considerations of the battery's state of health (e.g., aging effects). Specifically, we believe it would be worth exploring a pre-trained model using our system identification framework, followed by iterative updates employing recursive least squares techniques to account for state of health and/or aging dynamics. Furthermore, we intend to conduct empirical research to assess the impact of temperature on battery performance, recognizing its significant influence on modifying battery parameters.

REFERENCES

[1] A. Contini and A. Farinelli, "Coordination approaches for multi-item pickup and delivery in logistic scenarios," *Robot. Auton. Syst.*, vol. 146, no. C, dec 2021.

[2] S. Dong, K. Xu, Q. Zhou, A. Tagliasacchi, S.-Q. Xin, M. Nießner, and B. Chen, "Multi-robot collaborative dense scene reconstruction," *ACM Transactions on Graphics*, vol. 38, pp. 1–16, 07 2019.

[3] A. Denker and M. C. İşeri, "Design and implementation of a semi-autonomous mobile search and rescue robot: Salvor," in *2017 International Artificial Intelligence and Data Processing Symposium (IDAP)*, 2017, pp. 1–6.

[4] M. Partovibakhsh and G. Liu, "An adaptive unscented Kalman filtering approach for online estimation of model parameters and state-of-charge of lithium-ion batteries for autonomous mobile robots," *IEEE Transactions on Control Systems Technology*, vol. 23, no. 1, pp. 357–363, 2015.

[5] A. A. Chellal, J. Lima, J. Gonçalves, and H. Megnafi, "Battery management system for mobile robots based on an extended Kalman filter approch," in *2021 29th Mediterranean Conference on Control and Automation (MED)*, 2021, pp. 1131–1136.

[6] H. Li, W. Zhang, B. Sun, J. Jiang, Z. Yin, J. Wu, and X. He, "Lithium-ion battery modeling under high-frequency ripple current for co-simulation of high-power dc-dc converters," *Journal of Energy Storage*, vol. 54, p. 105284, 2022.

[7] B. Morabito, R. Klein, and R. Findeisen, "Real time feasibility and performance of moving horizon estimation for Li-ion batteries based on first principles electrochemical models," in *2017 American Control Conference (ACC)*, 2017, pp. 3457–3462.

[8] X. Hu, D. Cao, and B. Egardt, "Condition monitoring in advanced battery management systems: Moving horizon estimation using a reduced electrochemical model," *IEEE/ASME Transactions on Mechatronics*, vol. 23, no. 1, pp. 167–178, 2018.

[9] Y. Hu and Y.-Y. Wang, "Two time-scaled battery model identification with application to battery state estimation," *IEEE Transactions on Control Systems Technology*, vol. 23, no. 3, pp. 1180–1188, 2015.

[10] X. Du, J. Meng, K. Liu, Y. Zhang, S. Wang, J. Peng, and T. Liu, "Online identification of lithium-ion battery model parameters with initial value uncertainty and measurement noise," *Chinese Journal of Mechanical Engineering*, vol. 36, no. 1, Jan. 2023. [Online]. Available: http://dx.doi.org/10.1186/s10033-023-00846-0

[11] D. Gandolfo, A. Brandão, D. Patiño, and M. Molina, "Dynamic model of lithium polymer battery – load resistor method for electric parameters identification," *Journal of the Energy Institute*, vol. 88, no. 4, pp. 470–479, 2015.

[12] L. Chen, W. Yu, G. Cheng, and J. Wang, "State-of-charge estimation of lithium-ion batteries based on fractional-order modeling and adaptive square-root cubature Kalman filter," *Energy*, vol. 271, p. 127007, 2023.

[13] M. Kwak, B. Lkhagvasuren, J. Park, and J.-H. You, "Parameter identification and SoC estimation of a battery under the hysteresis effect," *IEEE Transactions on Industrial Electronics*, vol. 67, no. 11, pp. 9758–9767, 2020.

[14] X. Chen, W. Shen, Z. Cao, and A. Kapoor, "A novel approach for state of charge estimation based on adaptive switching gain sliding mode observer in electric vehicles," *Journal of Power Sources*, vol. 246, pp. 667–678, 2014.

[15] B. Xia, X. Zhao, R. de Callafon, H. Garnier, T. Nguyen, and C. Mi, "Accurate lithium-ion battery parameter estimation with continuous-time system identification methods," *Applied Energy*, vol. 179, pp. 426–436, 2016.

[16] P. Malysz, J. Ye, R. Gu, H. Yang, and A. Emadi, "Battery state-of-power peak current calculation and verification using an asymmetric parameter equivalent circuit model," *IEEE Transactions on Vehicular Technology*, vol. 65, no. 6, pp. 4512–4522, 2016.

[17] A. Fotouhi, D. J. Auger, K. Propp, and S. Longo, "Accuracy versus simplicity in online battery model identification," *IEEE Transactions on Systems, Man, and Cybernetics: Systems*, vol. 48, no. 2, pp. 195–206, 2018.

[18] L. Zhang, X. Wang, M. Chen, F. Yu, and M. Li, "A fractional-order model of lithium-ion batteries and multi-domain parameter identification method," *Journal of Energy Storage*, vol. 50, p. 104595, 2022.

[19] M. Cai, W. Chen, and X. Tan, "Battery state-of-charge estimation based on a dual unscented Kalman filter and fractional variable-order model," *Energies*, vol. 10, no. 10, 2017.

[20] P. E. Jacob, S. M. M. Alavi, A. Mahdi, S. J. Payne, and D. A. Howey, "Bayesian inference in non-markovian state-space models with applications to battery fractional-order systems," *IEEE Transactions on Control Systems Technology*, vol. 26, no. 2, pp. 497–506, 2018.

[21] J. Tian, R. Xiong, W. Shen, J. Wang, and R. Yang, "Online simultaneous identification of parameters and order of a fractional order battery model," *Journal of Cleaner Production*, vol. 247, p. 119147, 2020.

[22] B. Wang, S. E. Li, H. Peng, and Z. Liu, "Fractional-order modeling and parameter identification for lithium-ion batteries," *Journal of Power Sources*, vol. 293, pp. 151–161, 2015.

[23] H. Rahimi-Eichi, F. Baronti, and M.-Y. Chow, "Online adaptive parameter identification and state-of-charge coestimation for lithium-polymer battery cells," *IEEE Transactions on Industrial Electronics*, vol. 61, no. 4, pp. 2053–2061, 2014.

[24] P. Rodríguez-Iturriaga, J. A. del Valle, S. Rodríguez-Bolívar, D. Anseán, J. C. Viera, and J. A. López-Villanueva, "A novel dual fractional-order extended Kalman filter for the improved estimation of battery state of charge," *Journal of Energy Storage*, vol. 56, p. 105810, 2022.

[25] J. Shen, Q. Wang, G. Zhao, Z. Ma, and Y. He, "A joint moving horizon strategy for state-of-charge estimation of lithium-ion batteries under combined measurement uncertainty," *Journal of Energy Storage*, vol. 44, p. 103316, 2021.

[26] *Maximum Power Estimation of Lithium-Ion Batteries Accounting for Thermal and Electrical Constraints*, ser. Dynamic Systems and Control Conference, vol. 2, 10 2013, v002T23A003.

[27] A. J. Gonzalez-Castellanos, D. Pozo, and A. Bischi, "Non-ideal linear operation model for Li-ion batteries," *IEEE Transactions on Power Systems*, vol. 35, no. 1, pp. 672–682, 2020.

[28] Q. Guo and R. E. White, "Cubic spline regression for the open-circuit potential curves of a lithium-ion battery," *Journal of The Electrochemical Society*, vol. 152, no. 2, p. A343, 2005.

[29] I. Petras, "Fractional-order nonlinear systems. modeling, analysis and simulation. beijing and springer," 2011.

[30] A. Alessandretti, S. Pequito, G. J. Pappas, and A. P. Aguiar, "Finite-dimensional control of linear discrete-time fractional-order systems," *Automatica*, vol. 115, p. 108512, 2020.

[31] M. Marsden, "Cubic spline interpolation of continuous functions," *Journal of Approximation Theory*, vol. 10, no. 2, pp. 103–111, 1974.

[32] "Chapter II the cubic spline," in *The Theory of Splines and Their Applications*, ser. Mathematics in Science and Engineering, J. Ahlberg, E. Nilson, and J. Walsh, Eds. Elsevier, 1967, vol. 38, pp. 9–74.

[33] M. Kupper, C. Funk, M. Eckert, and S. Hohmann, "Fractional extended and unscented kalman filtering for state of charge estimation of lithium-ion batteries," in *2018 Annual American Control Conference (ACC)*, 2018, pp. 3855–3862.